Materials & Design 232 (2023) 112149

Contents lists available at ScienceDirect

Materials & Design

journal homepage: www.elsevier.com/locate/matdes

Experimental and numerical analyses of the thermoplastic pultrusion of large structural profiles

Kirill Minchenkov [a,*], Sergey Gusev [a], Artem Sulimov [a], Omar Alajarmeh [b], Ivan Sergeichev [a], Alexander Safonov [a]

[a] Skolkovo Institute of Science and Technology, Center for Materials Technologies, Moscow, Russia
[b] University of Southern Queensland, Centre for Future Materials, Toowoomba Queensland, Australia

ARTICLE INFO

Keywords:
Fiber-Reinforced Materials
Thermoplastics
Pultrusion
Polypropylene
Glass Fiber
Finite Element Analysis

ABSTRACT

The selection of optimal process conditions is very important for the production of large pultruded thermoplastic profiles. This study investigates the influence of pulling speed on the temperature distribution and consolidation of glass fiber/polypropylene (GF/PP) preconsolidated tapes during thermoplastic pultrusion. For this purpose, several pultruded thermoplastic profiles with a cross-section of 75 mm × 3.5 mm were produced at various pulling speeds, and their cross-sections were studied under a microscope. In addition, a 3D numerical model was developed to analyze the influence of the pulling speed on the temperature distribution and to predict the consolidation of the tapes. Full consolidation of the tapes was observed in the profiles produced at a pulling speed of 0.2 m/min. The profiles produced at a pulling speed of 0.4 m/min contained unconsolidated tape, which resulted in reduced flexural, tensile, and compressive strengths by as much as 43%, 15%, and 23%, respectively. The results of the simulations and microscopic investigations show that the GF/PP tapes consolidate at temperatures above the Vicat softening temperature. Finally, a GF/PP tube with dimensions of 50 mm × 40 mm × 5 mm was produced using the optimum pulling speed and temperature determined using the developed 3D model. These results provide valuable insight into the design of thermoplastic pultrusion regimes.

1. Introduction

Structural components made of fiber-reinforced polymers have been widely applied in aerospace [1], civil [2,3], energy systems [4,5], and marine engineering [6] owing to their high specific strength and stiffness [7,8], improved durability [9], excellent fatigue [10,11], and corrosion resistance [12,13]. One of the most efficient composite-manufacturing methods is the pultrusion process [14]. In the conventional pultrusion process, the fiber reinforcement passes through an impregnation bath with a thermosetting polymer and is then fed into a heated die block, where the polymerization process occurs, and a profile assumes its shape. A polymerized profile with a constant cross-section exits the die block and is cut to the desired length. Pultrusion can also be used to manufacture composites using thermoplastic matrices. Because no polymerization occurs in thermoplastic pultrusion, the polymer is heated to impregnate the fibers; the obtained profile is then cooled to fix its shape. The use of thermoplastic polymers instead of thermosetting polymers offers the benefits of nearly indefinitely long storage of source materials [15], use of welded joints [16], material recycling [17], and reduced harmful effects on the environment owing to the absence of volatile organic compounds such as epichlorohydrin and styrene [18]. However, the major problem with thermoplastic matrices is their high melt viscosity, which impedes the impregnation of fiber reinforcement. The presence of unimpregnated reinforcement fibers impairs the mechanical and physical performances of the produced material [19]. To facilitate the impregnation of reinforcement in thermoplastic pultrusion, the process uses prepreg materials such as commingled yarns [20], towpregs [21], and preconsolidated tapes (PCT) [22], where the reinforcing fibers are in close contact with the polymer matrix. The use of PCT enables the separation of the impregnation of the fibers from the pultrusion process.

Currently, thermosetting pultrusion is used to manufacture complex shape profiles such as boxes [23], L-shaped [24,25], I-beam [26], and U-shaped [27] profiles. Large profiles of fiber-reinforced thermoset plastics have been used to produce large-scale frames [28], vehicular [29], pedestrian bridge decks [30,31], bridge enclosures, carwash porches

* Corresponding author.
E-mail address: kirill.minchenkov@skoltech.ru (K. Minchenkov).

https://doi.org/10.1016/j.matdes.2023.112149
Received 20 February 2023; Received in revised form 7 June 2023; Accepted 6 July 2023
Available online 8 July 2023

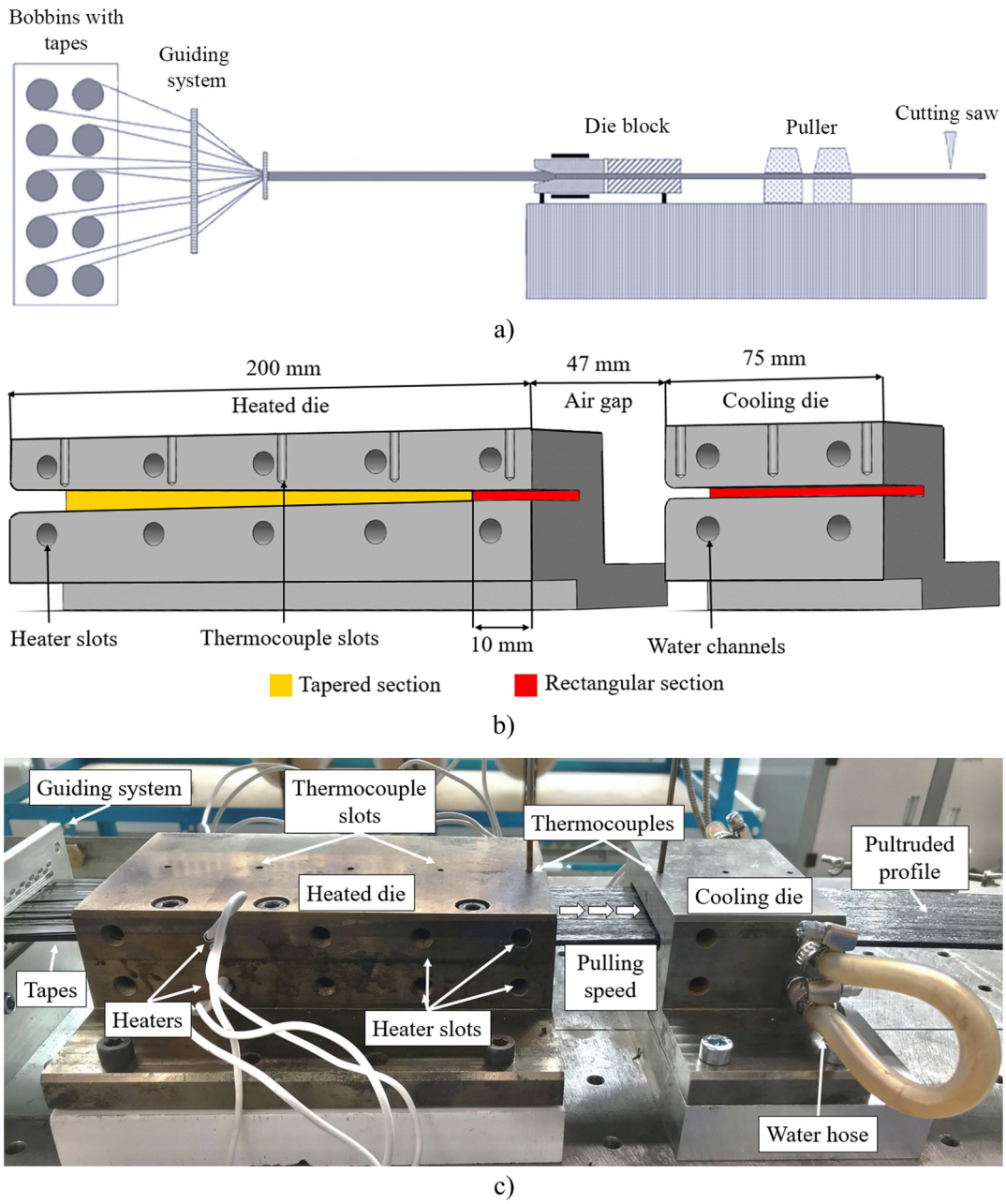

Fig. 1. Pultrusion of thermoplastic strip profile of 75 mm × 3.5 mm: (a) schematic of the thermoplastic pultrusion process, (b) the section of the die block CAD model by the symmetry plane, (c) the die block during pultrusion.

[32], elevator rods [33], and vehicle components [34]. Unfortunately, the production of large, complex-shaped thermoplastic profiles is poorly represented in the scientific literature and engineering practice. Continuous thermoplastic pultrusion can be used to produce rods of up to Ø 20 mm for use in high-voltage overhead power lines [35] and thermoplastic strip profiles of 30 mm, 75 mm wide [36,37] and 3.5 mm thick [38]. The batch pultrusion process can be used to produce rods up to 40 mm in size [39].

Various mathematical models have been developed for thermoplastic pultrusion to analyze the resin flow, impregnation, crystallization, heat transfer, and pulling speed [40]. A numerical model of impregnation based on the existing Newtonian and power-law models was proposed by Sala et al., [41] to describe the viscosity of a polymer matrix. Miller et al., [42] proposed a towpreg impregnation model that considered capillary forces. Dual-scale porous media flow models were developed by Kim et al., [43] to describe the impregnation of reinforcements during the pultrusion process. Koubaa et al., [44] proposed a one-dimensional (1D) model of the resin flow and impregnation for straight and tapered die blocks based on the Navier–Stokes equation and Darcy's law. Carlsson, Astrom, and Pipes [45,46] used simulations to solve several problems related to heat transfer, pulling force, and crystallization kinetics. Babeau et al., [47] used 2D heat transfer models and experimental methods to investigate heat transfer during pultrusion. Volk et al., [39] used the finite element analysis methods and models proposed by Kim and Astrom to solve the 2D heat transfer problem and determine the optimum process parameters for the pultrusion of rods. Compared to thermoplastic pultrusion, 3D models of the strain–stress state and heat transfer to evaluate the pulling force during the pultrusion of complex shape profiles have been developed for thermoset pultrusion [48,49]. Therefore, further development in thermoplastic pultrusion and the production of large, complex thermoplastic profiles with high mechanical properties will require mathematical

models to describe the physical phenomena and postulate process quality criteria.

This study investigated the influence of pulling speed on the temperature distribution inside the die block and on the consolidation of PCT tapes in a flat pultruded profile of 75 mm × 3.5 mm. To analyze the relationship between the pulling speed and temperature distribution, a 3D model was developed using the ABAQUS finite element analysis suite. The model was experimentally validated using thermocouples to monitor the temperature inside the profile. The simulation results and profile cross-section micrographs showed that the consolidation of the GF/PP tapes occurred above the Vicat Softening Temperature (A50). The developed FE model was adapted for the pultrusion of a rectangular tube with dimensions of 50 mm × 40 mm × 5 mm and used to determine the process regimes. Pultruded thermoplastic tubes can be used as reinforcing elements for door and window structures made of polyvinyl chloride (PVC).

2. Materials and methods

2.1. Pultrusion setup

A flat thermoplastic profile with a cross-section of 75 mm × 3.5 mm was manufactured from PCT tapes using a Pultrex Px500-6T pultrusion machine (Pultrex, UK). Initially, tapes were fed through the guiding system into the heated die block where they were heated and assumed the shape of the profile. Then, the material was fed into the cooling die, where it was cooled and hardened. Finally, the profile was cut into sections of the desired length using a cutting saw. Fig. 1(a) shows a schematic of the thermoplastic pultrusion process and its main steps.

In this study, we used a GF/PP preconsolidated tape produced by ApATeCh (Russia). The tapes are 4.83 mm × 0.66 mm and consist of 2400 TEX unidirectional glass fiber rovings and a Moplen RP348U polypropylene matrix (Lyondell Basell, Netherlands). According to data provided by the manufacturer, the matrix mass fraction was 36.8% [50].

The temperature of the heating platens was set at 200 ± 10 °C. In the steady state process, the temperature of the cooling die was maintained at 60 ± 10 °C. The temperature inside the composite material was measured using embedded bare-wire thermocouples connected to a pultrusion machine to record the temperature data. The thermocouples were placed between the tapes before the guiding system. The exact positions of the thermocouples were determined after the experiment because the thermocouples could move from the initial position owing to the mass flow of the melt.

The die block consisted of a heated die (200 mm × 115 mm × 60 mm) and a cooling die (75 mm × 115 mm × 60 mm) made of steel with a chrome coating on the cavity surfaces with an air gap between the dies. Fig. 1(b) shows a section of the die block based on a symmetry plane. The die block was heated using cylindrical heaters inserted into through slots on the sides of the forming die. The die was subsequently cooled in water. Thermocouples were installed in slots on the upper sides of the die blocks for monitoring the temperature. The cavity of the heated die has two zones: a straight one (with parallel walls) with a section of 75 mm × 3.5 mm, and the tapered one with a taper angle of 0.72°. The cavity of the cooling die has a rectangular cross-section (75 mm × 3.5 mm) over the entire length of the die. The die block during pultrusion of the strip profile is depicted in Fig. 1(c).

2.2. 3D numerical simulation of heat transfer

A 3D simulation was performed to analyze the temperature distribution over the die blocks and inside the composite material during pultrusion under various heating conditions and pulling speeds. Temperature distribution data were used to predict the consolidation of tapes inside the composite material and determine the maximum allowable pulling speed. The composite material with the tape used in the simulations was represented by a single transversely isotropic solid body. The consolidation of the tape into the composite profile was ignored in the simulation. The axis of anisotropy coincides with the OX axis of the Cartesian coordinate system, with the OY and OZ axes lying on the cross-sectional plane of the profile. The heated and cooled dies were represented by an isotropic solid body.

A numerical simulation of the heat transfer was performed based on the equations of heat transfer, which, in the case of thermoset pultrusion, can be expressed as follows [51]:

$$\rho_c Cp_c\left(\frac{\partial T}{\partial t}+u\frac{\partial T}{\partial x}\right)=k_{x,c}\frac{\partial^2 T}{\partial x^2}+k_{y,c}\frac{\partial^2 T}{\partial y^2}+k_{z,c}\frac{\partial^2 T}{\partial z^2}+q \tag{1a}$$

$$\rho_d Cp_d\frac{\partial T}{\partial t}=k_{x,d}\frac{\partial^2 T}{\partial x^2}+k_{y,d}\frac{\partial^2 T}{\partial y^2}+k_{z,d}\frac{\partial^2 T}{\partial z^2} \tag{1b}$$

where T is the temperature, t is the time, u is the pulling speed, ρ is the density, Cp is the specific heat, k_x, k_y, and k_z are the thermal conductivities along x, y, and z directions, respectively (x coincides with pulling direction, y and z coincide with the transverse directions), and q is the internal heat generation due to exothermic reaction of the epoxy resin. Subscripts c and d correspond to the composite and die, respectively. We consider thermoplastic pultrusion to be a steady-state process; therefore, the time derivative of the temperature on the left side of the equation can be neglected. No polymerization reaction occurred, and the heat generated during the exothermic reaction on the right side of the equation was transformed to zero. Thus, the steady-state heat transfer equations for thermoplastic pultrusion can be expressed as follows:

$$\rho_c Cp_c u\frac{\partial T}{\partial x}=k_{x,c}\frac{\partial^2 T}{\partial x^2}+k_{y,c}\frac{\partial^2 T}{\partial y^2}+k_{z,c}\frac{\partial^2 T}{\partial z^2} \tag{2a}$$

$$0=k_{x,d}\frac{\partial^2 T}{\partial x^2}+k_{y,d}\frac{\partial^2 T}{\partial y^2}+k_{z,d}\frac{\partial^2 T}{\partial z^2} \tag{2b}$$

The temperature inside the heater slots was approximated as constant because it was controlled by thermocouples, and the temperature fluctuations were rather small. The temperature was assumed to be constant at the entrance of the heated die block. The convective heating of the incoming tapes was disregarded because the pultrusion speed was sufficiently high. The temperatures of the heated and cooling slots and composite material at the entrance to the heated die are given by Equation (3) for a constant surface temperature as follows:

$$T|\Omega = T_{surf}(x) \tag{3}$$

where T_{surf} is the surface temperature, Ω is the surface with a constant temperature. Because the contact between the moving composite material and die block is imperfect, thermal contact resistance exists. Considering the thermal contact resistance, the boundary condition between the composite and die block was modeled through the convective boundary condition [52] using Equation (4):

$$k\frac{\partial T}{\partial n}\Big|\Omega = -h_{die}(x)\bullet(T-T_{die}(x)) \tag{4}$$

where T is the temperature, k is the conductivity, Ω is the heat transfer area, h_{die} is the coefficient of heat transfer between the die block and composite material, T_{die} is the temperature of the die block cavity. The heat transfer between the ambient air and die block, as well as between the ambient air and composite material, is given by the equations of convective boundary conditions (5), as follows:

$$k\frac{\partial T}{\partial n}\Big|\Omega = -h_{air}(T-T_{air}) \tag{5}$$

where h_{air} is the coefficient of convective heat transfer between the ambient air and die surface, as well as between the ambient air and surface of the composite material, T_{air} is the temperature of the ambient air.

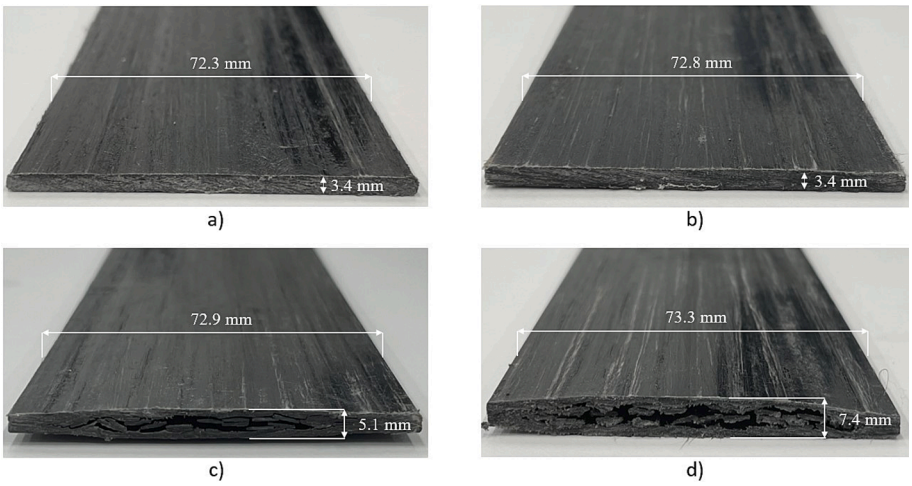

Fig. 2. Pultruded thermoplastic profiles produced at different pulling speeds: (a) V02, (b) V04, (c) V06, (d) V08.

2.3. Material characterization

To determine the heat capacity and conductivity of the produced material, a series of tests were performed in accordance with ISO 22007–4, at an LFA 457 laser flash analyzer (Netzsch, Germany).

The melting temperature of the polymers was determined using a DSC-60 Plus differential scanning calorimeter (Shimadzu, Japan). The measurements were conducted in the temperature range of 25–200 °C, at the heating rate of 5 °C/min, with an inert gas flow rate of 60 mL/min.

The mechanical tests were conducted using an Instron 5969 testing machine (Instron, USA). Specimens for mechanical testing were prepared at the CNC milling machine. Tensile, flexural, and compression tests were performed in accordance with the ISO 527, ASTM D790-02, and ASTM D6641 procedures, respectively. The geometry of the specimens used to determine the tensile properties in the fiber direction was adopted by Novo et al., [53].

An Axio Scope A1 optical microscope (Zeiss, Germany) was used to study the cross-section of the material. The specimens were ground and polished using a MetPrep 3 PH-3 grinder (Allied, USA). A polishing suspension with a particle size of 6 μm was used to complete the polishing.

3. Results

3.1. Manufactured materials

Fig. 2 shows the pultruded thermoplastic laminates produced at four different pulling speeds (0.2, 0.4, 0.6, and 0.8 m/min). The profiles are marked accordingly (V02, V04, V06, and V08). On the surface of the V02 specimen, matte and glossy regions were observed, with broken glass fibers visible on the matte surfaces. During visual inspection of the V04 specimen without optical magnifiers, the unconsolidated tape was not observed. The V04 specimen exhibits a glossier surface as compared to the surface of the V02 specimen. The cross-section of the V06 specimen exhibited a glossy surface with visibly broken fibers. No unconsolidated tapes can be observed at the side edges, in contrast to the central part of the cross-section, where separate unconsolidated tapes are visible. The V08 specimen had the glossiest surface among all specimens. The consolidated tape can only be observed at the periphery of the profile, and the thickness of the consolidated shell is equal to that of a single tape. The unconsolidated tape was observed in the peripheral and central regions of the V08 specimen.

The relationship between the high pulling speed and glossy surfaces of specimens V06 and V08 was also studied. The matrices of these specimens only melted on the surface and did not impregnate the material. With an increase in the pulling speed, the pressure increased; thus, the roughness of the surface decreased, and the material became glossy. The same effect was reported by Astrom et al., [54].

As the V08 specimen had more unconsolidated tapes than the V06 specimen, only specimens V02, V04, and V06 were used for the analysis.

3.2. Model validation and simulation results

The Abaqus FEA suite is used to solve the 3D heat transfer problem. The movement of the composite material was expressed in terms of the mass flow rate. The mass flow rate values in the x-, y-, and z-directions were set at each node of the composite material mesh. The values were written in the input file (inp) of Abaqus after the keyword “mass flow

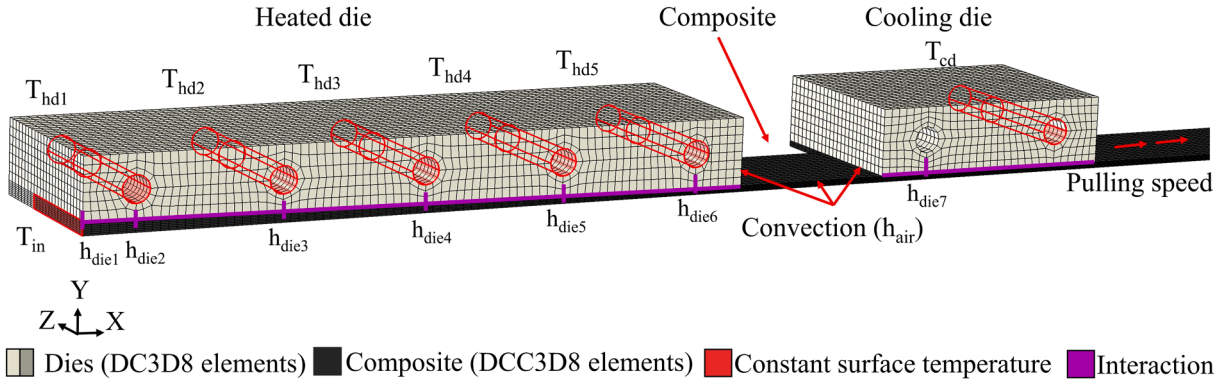

Fig. 3. FE model of the die block and composite material.

Table 1
Model parameters.

Parameter	Symbol	Value	Units	Source
Thermal conductivity of the composite				
• in the transverse direction	$k_{y.c}, k_{z,c}$	0.35	W/(m·°C)	a
• in the longitudinal direction	$k_{x,c}$	0.56	W/(m·°C)	a
Thermal conductivity of the die block	$k_{x,d}, k_{y.d}, k_{z,d}$	47	W/(m·°C)	c
Specific heat of the composite				
• at 20 °C	C_p	1044	J/(kg·°C)	a
• at 110 °C	C_p	1386	J/(kg·°C)	a
Coefficient of convective heat transfer between the ambient air and profile and between the ambient air and die block	h_{air}	10	W/(m^2·°C)	[56]
Coefficient of convective heat transfer between the die block and profile				
• at x = 15	h_{die1}	0.5, 1*	W/(m^2·°C)	b
• at x = 57.5	h_{die2}	1.5	W/(m^2·°C)	b
• at x = 100	h_{die3}	1.5	W/(m^2·°C)	b
• at x = 142.5	h_{die4}	200, 170*	W/(m^2·°C)	b
• at x = 185	h_{die5}	280, 450*	W/(m^2·°C)	b
• at x = 190	h_{die6}	320, 500*	W/(m^2·°C)	b
• at x = 307.5 (in cooling die)	h_{die7}	2000	W/(m^2·°C)	b
Temperature at the die block entrance	T_{in}	25	°C	c
Temperature at the 1st heating zone (x = 15)	$T_{hd}1$	200	°C	c
Temperature at the 2nd heating zone (x = 57.5)	$T_{hd}2$	200	°C	c
Temperature at the 3rd heating zone (x = 100)	$T_{hd}3$	200	°C	c
Temperature at the 4th heating zone (x = 142.5)	$T_{hd}4$	205	°C	c
Temperature at the 5th heating zone (x = 185)	$T_{hd}5$	195	°C	c
Temperature at the cooling zone (x = 307.5)	T_{cd}	52	°C	c
Temperature of the ambient air	T_{air}	25	°C	c
Polypropylene melting temperature	–	150	°C	a
Polypropylene Vicat softening temperature	–	130	°C	[57]
Density of the composite	ρ	1532	kg/m^3	a

a: determined from testing; b: assumed value; c: measured value. * Only for the pultrusion at a pulling speed of 0.6 m/min.

rate" through a python script. The mass flow of the material at the entrance and exit of the die block was assumed to be constant. The geometry of the composite material in the model repeated the geometry of the internal cavity of the die block and had tapered and rectangular regions. Therefore, the area of the cross-section through which the material passes can be expressed as a variable depending on the coordinate on the x-axis (pulling direction). Thus, the density of the material in the tapered part of the die block can be expressed by the linear law as the ratio of the profile cross-section (75 mm × 3.5 mm) to the area of the mass flow cross-section. The lowest density value of the composite set at the heated die entrance was calculated by multiplying the ratio (0.42) between the outlet and inlet cross-sections of the die. Furthermore, the specific heat of the composite material varied with temperature. This effect was simulated and approximated as a linear function based on two measured values.

Fig. 3 shows the finite element model of the die block. Owing to the symmetry, only a quarter of the die block was modeled for the computations. The heating temperature was set at the internal surfaces of the heater slots (T_{hd1} −T_{hd5}). The temperature of the tape at the die entrance was set at the surface of the composite material (T_{in}). The cooling-die temperature was set to that of the water channel (T_{cd}). An inverse modeling procedure (i.e., curve fitting) was performed to obtain the same temperature profiles as the experimental and simulation data. Six convective heat transfer coefficient values were assumed by minimizing the difference between the experimental and simulated data, similar to the study by Baran et al., [55].

The composite material was modeled using DCC3D8 linear hexahedral elements with convection, making it possible to set the mass flow. The composite material width (37.5 mm) in the model was set to 16 finite elements, and the thickness (1.75 mm) was set to eight elements. The length of the composite material inside the heated die (200 mm) was set as 84 finite elements. The length of the material between the dies (47 mm) was set as 20. The length of the composite material inside the cooling die (75 mm) was set to 30 finite elements. After cooling die, the length of the composite material (350 mm) was set to 146. DC3D8 linear hexahedral elements were used for the die blocks. Table 1 lists all the parameters used in the modeling.

The results of the heat transfer simulation for the pultrusion at pulling speeds of 0.2, 0.4, and 0.6 m/min are shown in Fig. 4(a), 4(b), and 4(c), respectively. Fig. 4(a)–(c) shows the regions with the highest temperatures of the finite elements located at the depth of the thermocouple. The 3D finite element model of the heat transfer was experimentally validated at pulling speeds of 0.2, 0.4, and 0.6 m/min. Fig. 4(d) shows the temperature evolution observed in the simulations and experiments as a function of the position coordinates. The simulation results are indicated by the colored dashed lines. Values obtained with bare-wire thermocouples are indicated by the colored dotted lines. The position of the thermocouple in the cross-section of the profile is shown in the bottom-right corner of the plot. The temperature values obtained by the simulation were taken from points located along the path of the movement of the thermocouples during the experiment. The red horizontal dashed lines indicate a melting temperature of 150 °C and a Vicat softening temperature (A50) of 130 °C [57]. The black vertical dashed lines indicate the boundaries between the heated and cooled dies.

The experimental data are in good agreement with the simulation results at all pulling speeds. The validated model was used to determine the highest temperature in the profile and temperature distribution over the profile during pultrusion. Fig. 5 shows the temperature distribution over the cross-section of the profile in the region with the highest profile temperature. The black line shows the isosurface corresponding to the melting temperature and the white line shows the isosurface corresponding to the VST temperature.

Only the V02 specimen was heated to the melting temperature over the entire cross-section. The V04 specimen reached the melting temperature only at the periphery of the profile; the material in the inner part of the profile did not reach the VST temperature. The temperature of the V06 specimen reached the melting point, and the VST temperature was recorded only at the periphery of the profile.

3.3. Morphological analysis

Fig. 6(a) shows a micrograph of the tape used in the pultrusion process. The fibers in the tape were assembled in bundles. The cross-section of the tape contained unimpregnated regions, pores, and regions of the matrix without reinforcing fibers. Fig. 6(b) shows micrographs of the central and peripheral regions of the V02 specimen. The V02 specimen consisted of fully consolidated tapes with no unconsolidated tapes visible in the cross-section. The fibers were assembled into bundles, repeating the tape shape. The matrix between the fiber bundles contained no reinforcing fibers. Unimpregnated fibers and pores were

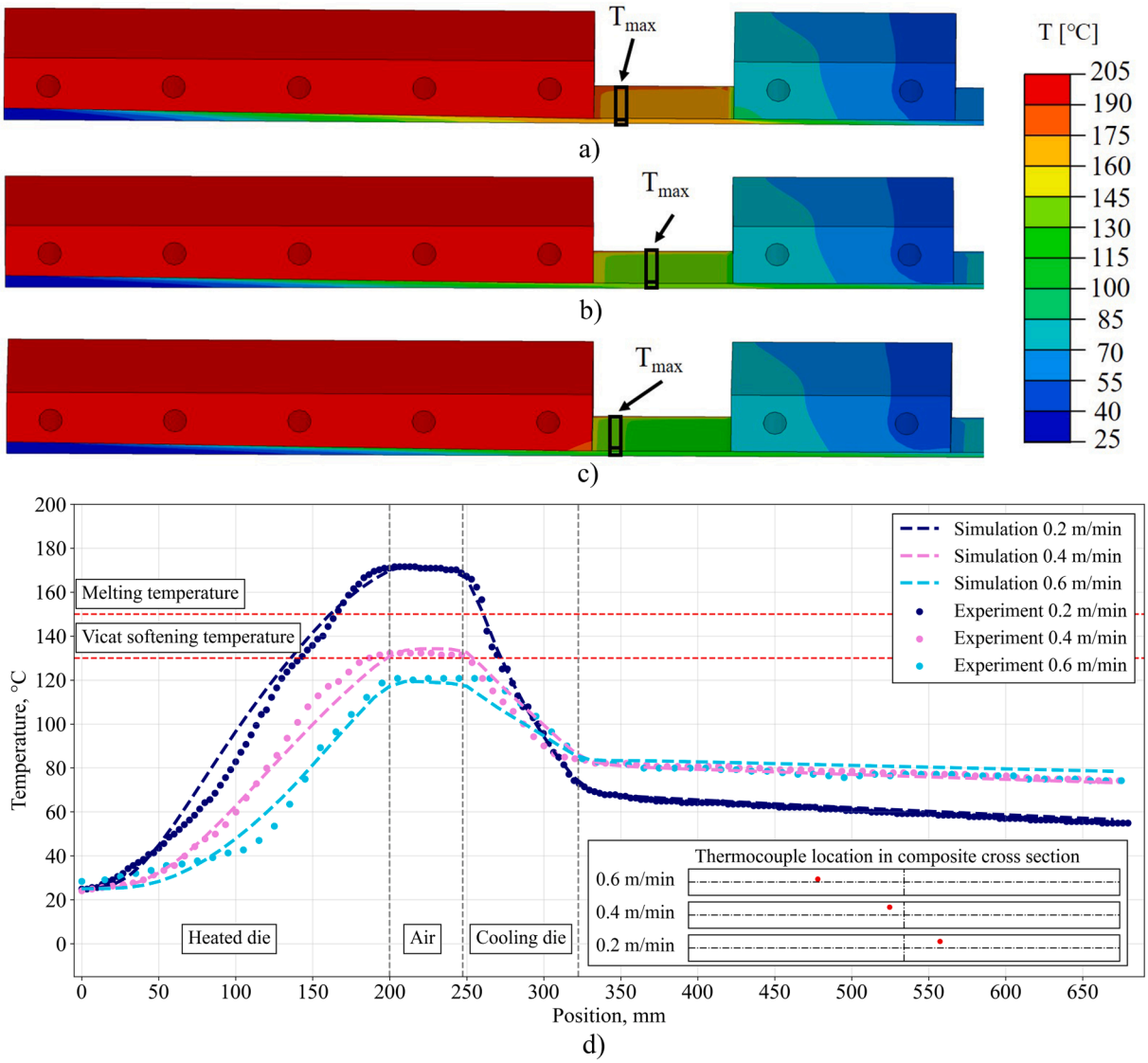

Fig. 4. Results of heat transfer simulation during pultrusion at pulling speeds of (a) 0.2 m/min, (b) 0.4 m/min, (c) 0.6 m/min (arrows show regions with the highest temperature of finite elements located at the depth of the thermocouple), (d) the temperature of the profile as the function of its position in the die block (based on experimental data and simulation results).

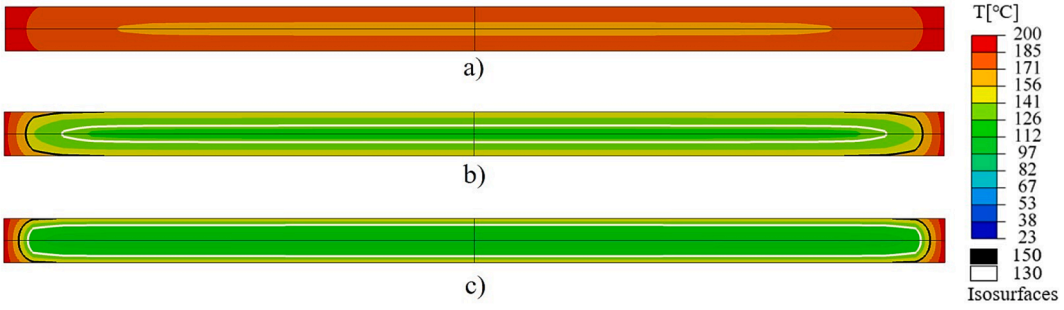

Fig. 5. Temperature of material in the region of the maximum heat: (a) V02, (b) V04, (c) V06.

observed at the center of the fiber bundles. Fig. 6(c) shows micrographs of the central and peripheral regions of the V04 specimen. Regions of the consolidated tape can be observed at the periphery of the specimen. In the central part of the profile, the cross-sectional tape remained unconsolidated. Several voids formed by unconsolidated tape can be found on the sides of the profile, with the nearest void located at a distance of 5.2 mm from the left edge of the profile. The void nearest to the upper boundary of the profile was found at a distance of 1.1 mm from the upper edge of the profile. The V04 specimen exhibited a higher porosity than the V02 specimen. Thus, we can see that the composite material produced at the pulling speed of 0.4 m/min and the temperature of the heated die of 200 °C contained voids resulting from the insufficient

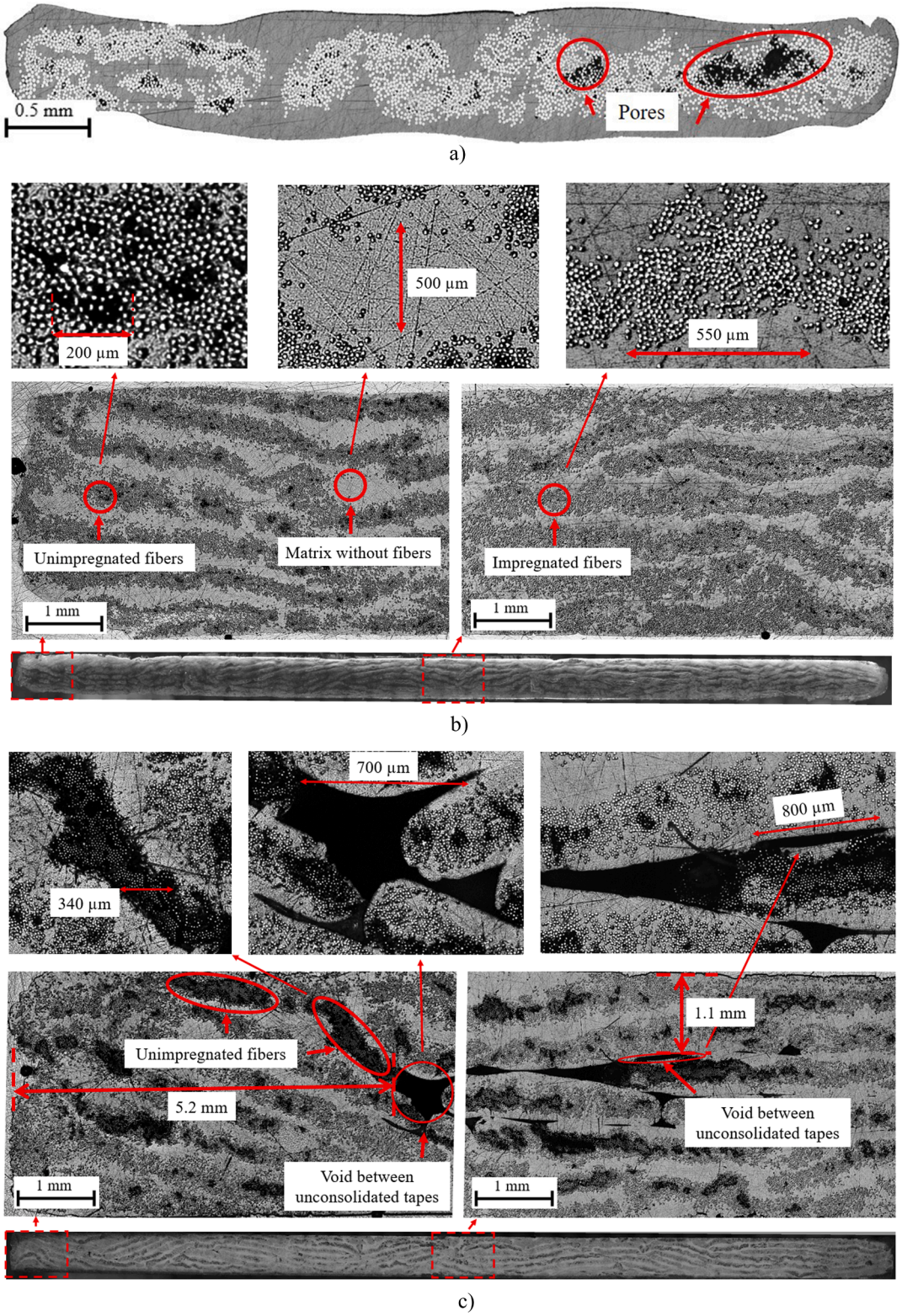

Fig. 6. Microstructure of specimens: (a) tape used for profile manufacture, (b) V02 specimen, (c) V04 specimen.

consolidation of tapes. At the pulling speed of 0.2 m/min and the die temperature of 200 °C, all tapes in the profile are fully consolidated.

The relationship between the microstructures of the specimens and the simulation results was established. The V02 profile could reach the melting temperature, which resulted in full consolidation of the tapes in the profile. In the V04 profile, the melting temperature was near the profile surface. The VST was reached at a depth equal to the thickness of the two tapes from the profile surface, and the tapes in this region were consolidated. The core of the V04 profile did not reach the VST, and the tape remained unconsolidated. Moreover, the V02 profile had fewer unimpregnated fibers than the V04 profile. According to the simulation results, the temperature of the V06 profile did not reach a VST point deeper than the tape thickness. Thus, the tapes consolidated above the VST. Heating the entire profile to the melting temperature, improving

Table 2
Mechanical properties of pultruded GF/PP profiles made of tapes.

GF/PP material studied	Current study V02	Current study V04	PCT laminate by Novo et al. [53]	ComTape laminate by Esfandiari [58]
Flexural modulus [GPa]	26.8 ± 0.5	25.7 ± 2.9	16.8 ± 1.5	20.9 ± 0.9
Flexural strength [MPa]	411.0 ± 27.9	235.0 ± 91.2	329.0 ± 30.0	416.6 ± 13.0
Tensile modulus [GPa]	28.7 ± 0.3	25.2 ± 0.7	21.4 ± 1.5	26.0 ± 0.9
Tensile strength [MPa]	659.8 ± 28.4	561.0 ± 34.9	355.8 ± 53.2	–
Compression modulus [GPa]	27.2 ± 2.5	25.9 ± 3.7	–	–
Compression strength [MPa]	202.9 ± 7.9	154.8 ± 25.0	–	–
Cross-sectional dimensions of a composite profile [mm × mm]	75 × 3.5	75 × 3.5	20 × 3	20 × 2
Pulling speed [m/min]	0.2	0.4	0.2	0.2

the impregnation of fibers inside the tape and reducing the porosity in the produced profile.

3.4. Mechanical properties

Mechanical tests were conducted only on specimens V02 and V04, as it was impossible to fabricate specimens V06 and V08 because of the presence of a large amount of unconsolidated tape in the profiles. The results of the mechanical tests are presented in Table 2. A comparison of V02 and V04 test results showed that an increase in pulling speed resulted in a slight reduction in flexural, tensile, and compression moduli by as much as 4%, 11%, and 5%, respectively. In addition, the reductions in flexural, tensile, and compressive strengths were 43%, 15%, and 23%, respectively. Further, specimen V04 exhibited a higher standard deviation. Thus, the presence of unconsolidated tape, caused by insufficient heating of the material at high pulling speeds, degrades the mechanical performance of the produced composite. For comparison, Table 2 also shows (*in italics*) the best mechanical properties of the pultruded thermoplastic profiles produced from GF/PP tapes found in the available literature [54,58].

3.5. Pultrusion of the rectangular tube and implication for design

Based on the validated model and tape consolidation temperature obtained, the optimum pulling speed was selected to produce a thermoplastic tube. A solid die-block assembly with integrated heating and cooling zones was used to produce the tube profile. The internal cavity of the die block has a 450 mm long tapered zone with a taper angle of

Table 3
Boundary condition parameters for thermoplastic tube pultrusion.

Coefficient of convective heat transfer between the die block and the profile			
• at x = 197	h_{die}	0.5	W/(m^2.°C)
• at x = 245	h_{die}	1.5	W/(m^2.°C)
• at x = 312	h_{die}	1.5	W/(m^2.°C)
• at x = 370	h_{die}	200	W/(m^2.°C)
• at x = 439	h_{die}	280	W/(m^2.°C)
• at x = 450	h_{die}	320	W/(m^2.°C)
• at x = 560–600 (in the cooling die)	h_{die}	2000	W/(m^2.°C)
Temperature at the die block entrance	T_{in}	25	°C
Heating temperature	T_{hd}	220	°C
Cooling temperature	T_{cd}	80	°C

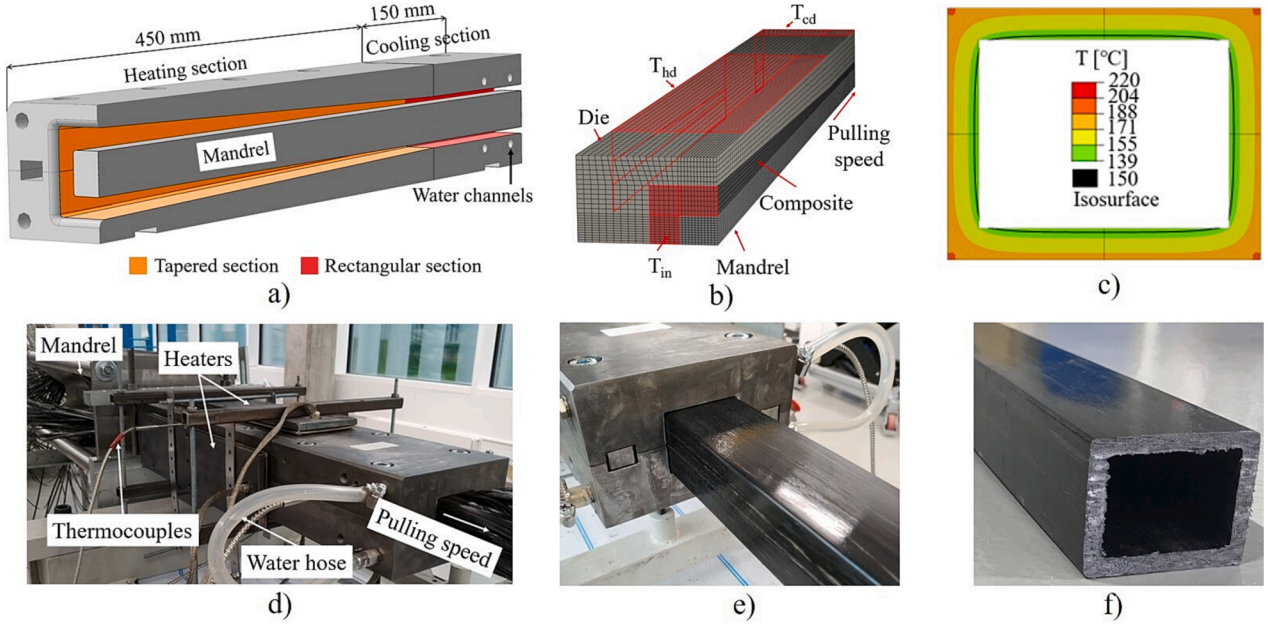

Fig. 7. Heat transfer simulation and pultrusion of the rectangular thermoplastic tube, based on the simulation results: (a) section of the CAD model of the die block based on the symmetry plane, (b) FE model of thermoplastic tube pultrusion, (c) distribution of temperatures over the profile produced at the pulling speed of 0.1 m/mm, (d) die assembly, (e) profile at the die block exit, (f) produced profile.

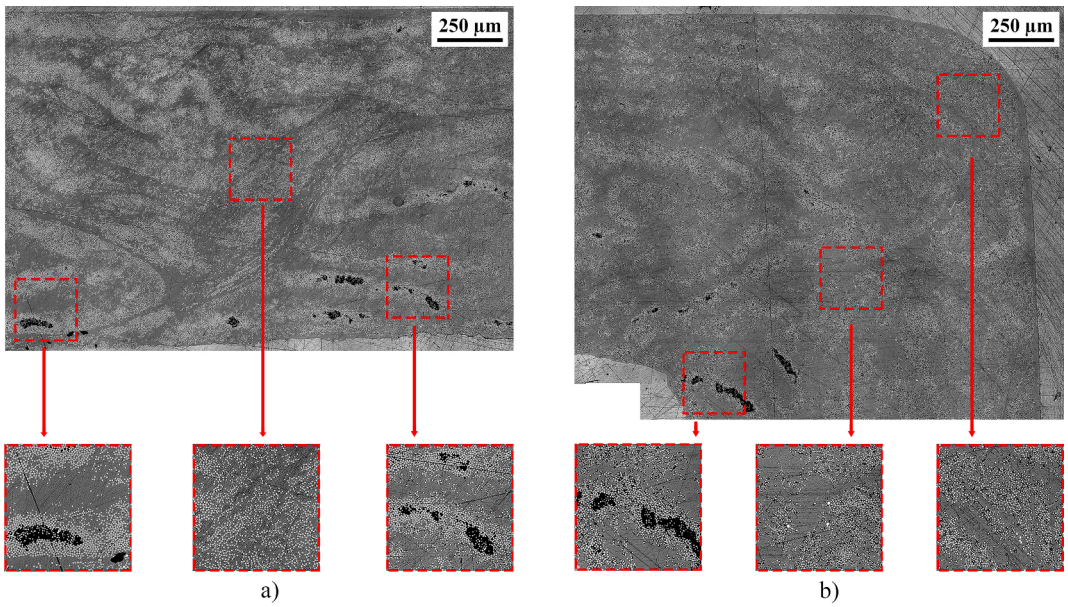

Fig. 8. Micrographs with zoomed areas of: (a) edge section of the tube, (b) corner section of the tube.

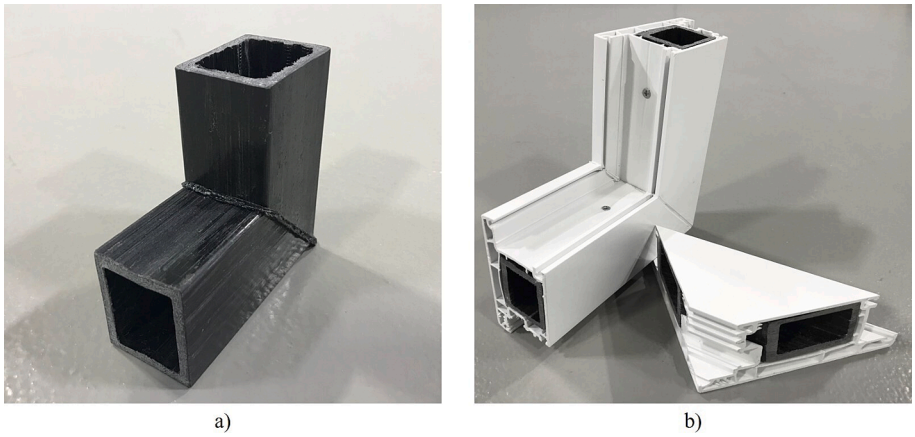

Fig. 9. Use of thermoplastic composite tube as the reinforcing element in the design of window and door structures: (a) welded angle joint of thermoplastic tubes, (b) the assembly of the thermoplastic tube and PVC profile.

1.27° and a 150 mm long constant section zone (see Fig. 7 (a)). The die block was heated using flat rectangular heating plates installed on the sides of the die block. The die block was equipped with a water-cooling system for cooling. To form the internal cavity in the profile, the die block was equipped with a mandrel that was not connected to heating and cooling systems. A mandrel was installed at the die block entrance. The heating and cooling temperatures were monitored using thermocouples installed in special slots on the sides of the die block.

The approach described in Section 2.2 (see Fig. 7(b)) was used to simulate the pultrusion of a thermoplastic tube. The material properties, boundary, and contact conditions were set based on Equations 2–5. However, the 3D heat transfer models used for the simulation of the tube and flat laminate pultrusion had different boundary surfaces. The parameters used as boundary conditions in the tube pultrusion simulations are listed in Table 3. Based on simulations, the maximum allowable pulling speed was determined such that the temperature of the profile at the die block exit exceeded the VST temperature. According to simulations, the maximum allowable pulling speed should not exceed 0.1 m/min at the heating temperature of 220 °C (see Fig. 7 (c)). The pulling speed of 0.15 m/min results in the internal part of the profile not being able to reach the VST temperature. Fig. 7(d)–(f) shows the fabrication of the pultruded tube from the preconsolidated tapes.

According to the simulation results, the region with the lowest temperature was located at the center of the tube wall. Fig. 8 shows micrographs of the magnified areas of the edge and corner sections of the tube. The cross-section was uniform with fully consolidated tapes. No pores were visible in the upper part of the section closest to the heater. However, pores were observed in the region that was in contact with the mandrel. The tapes in the tube-corner regions were fully consolidated.

A thermoplastic tube can be used to reinforce the window and door frame profiles made of PVC [59] (see Fig. 9). Thermoplastic tubes offer the benefit of a lower heat conduction coefficient. The use of a thermoplastic matrix offers the benefit of joining profile parts via welding. The design idea of the window and door structures based on a pultruded thermoplastic tube is shown in Fig. 9.

The effects of the pulling speed on the temperature distribution during the pultrusion of the thermoplastic profiles were investigated. A high pulling speed reduced the profile temperature during manufacturing. The GF/PP tapes consolidated above the Vicat softening temperature (A50). The tapes heated below the VST remained unconsolidated inside the profile, and the mechanical properties of the

composite profiles were reduced. Heating the material to its melting point during pultrusion reduced the number of pores in the tape and porosity of the profile. These results can be used in future designs of pultrusion regimes for manufacturing large structural profiles.

In future studies, the authors intend to study the influence of pressure inside the die block on the mechanical properties and morphology of pultruded thermoplastic profiles using the existing models of thermoplastic composite consolidation [60]. In addition to studying the influence of pressure, we intend to develop models of residual stresses and shape distortions during the thermoplastic pultrusion process. Similar models are available for thermosetting pultrusion, enabling the prediction of cracking, spring-in, and warpage in pultruded profiles [51,61,62]. We believe that future thermoplastic pultrusion models, together with process parameter optimization techniques [56] will make it possible to achieve the maximum production rate and produce thermoplastic profiles of more complex shapes. Pultrusion studies have also been conducted using thermoplastic tapes and pultruded profiles based on PEEK, carbon fibers, and nanotubes.

4. Conclusion

Experimental and numerical analyses of the thermoplastic pultrusion process based on GF/PP tapes were conducted to better understand the influence of pulling speed on the properties of the produced profiles. In the course of the study, the flat thermoplastic laminates of 75 mm × 3.5 mm were produced at pulling speeds of 0.2, 0.4, 0.6, and 0.8 m/min. The analysis showed that profiles produced at pulling speeds of 0.4, 0.6, and 0.8 m/min had unconsolidated tapes, which can be attributed to the high pulling speeds and, consequently, insufficient heating of the material. A 3D model was developed to analyze the temperature distribution as a function of the pulling speed. The model was experimentally validated using thermocouples to monitor the temperature inside the profile. The main outcomes of this study are summarized as follows:

- The micrographs and simulation results show that consolidation of the GF/PP tapes is possible at temperatures above the Vicat softening temperature. The tape heated below the VST remained unconsolidated inside the profile. Heating the material to its melting point during pultrusion reduces the number of pores in the tape and the porosity of the profile.
- The results of the mechanical tests show that an increase in pulling speed results in reduced flexural, tensile, and compression moduli by as much as 4%, 12%, and 5%, respectively, and in reduced flexural, tensile, and compression strengths by as much as 43%, 15%, and 23%, respectively.
- The developed 3D model for the pultrusion of the strip profile was successfully adopted to manufacture a tube with dimensions of 50 mm × 40 mm × 5 mm. Based on the tape consolidation criteria, pulling speed, and temperature obtained from the model, a thermoplastic tube was produced.

The results of this study provide insights into the future design of thermoplastic pultrusion regimes for manufacturing large structural profiles.

CRediT authorship contribution statement

Kirill Minchenkov: Investigation, Software, Data curation, Writing – original draft, Writing – review & editing. **Sergey Gusev:** Investigation, Resources. **Artem Sulimov:** Investigation, Data curation. **Omar Alajarmeh:** Investigation, Data curation, Resources, Funding acquisition. **Ivan Sergeichev:** Methodology, Funding acquisition, Software. **Alexander Safonov:** Supervision, Conceptualization, Writing – original draft, Writing – review & editing.

Declaration of Competing Interest

The authors declare that they have no known competing financial interests or personal relationships that could have appeared to influence the work reported in this paper.

Data availability

The authors are unable or have chosen not to specify which data has been used.

Acknowledgements

The authors would like to acknowledge the support provided by Russian Science Foundation (https://rscf.ru/en/project/21-19-00563/).

References

[1] E.C. Botelho, N. Scherbakoff, M.C. Rezende, A.M. Kawamoto, J. Sciamareli, Synthesis of polyamide 6/6 by interfacial polycondensation with the simultaneous impregnation of carbon fibers, Macromolecules 34 (2001) 3367–3375, https://doi.org/10.1021/ma000902k.
[2] L. Ding, L. Liu, X. Wang, H. Shen, Z. Wu, Effects of connecting materials on the static and fatigue behavior of pultruded basalt fiber-reinforced polymer bolted joints, Constr. Build. Mater. 273 (2021), 121683, https://doi.org/10.1016/j.conbuildmat.2020.121683.
[3] A. Moskaleva, A. Safonov, E. Hernández-Montes, Fiber-reinforced polymers in freeform structures: a review, Buildings 11 (2021) 1–27, https://doi.org/10.3390/buildings11100481.
[4] T. Starr, Pultrusion for engineers, Woodhead Publishing, Sawston, UK, 2000.
[5] D.S. Gemi, Ö.S. Şahin, L. Gemi, Experimental investigation of axial compression behavior after low velocity impact of glass fiber reinforced filament wound pipes with different diameter, Compos. Struct. 280 (2022) 114929, https://doi.org/10.1016/j.compstruct.2021.114929.
[6] F. Rubino, A. Nisticò, F. Tucci, P. Carlone, Marine application of fiber reinforced composites: a review, J. Mar. Sci. Eng. 8 (1) (2020) 26, https://doi.org/10.3390/JMSE8010026.
[7] Z. Guo, Y. Zhu, Y. Chen, Y. Zhao, Test on residual ultimate strength of pultruded concrete-filled GFRP tubular short columns after lateral impact, Compos. Struct. 260 (2021), 113520, https://doi.org/10.1016/j.compstruct.2020.113520.
[8] A. Moskaleva, S. Gusev, S. Konev, I. Sergeichev, A. Safonov, E. Hernandez-montes, Composite freeform shell structures: design, construction and testing, Compos. Struct. 306 (2023), 116603, https://doi.org/10.1016/j.compstruct.2022.116603.
[9] E. Madenci, Y. Onuralp Özkılıç, L. Gemi, Buckling and free vibration analyses of pultruded GFRP laminated composites: experimental, numerical and analytical investigations, Compos. Struct. 254 (2020) 112806, https://doi.org/10.1016/j.compstruct.2020.112806.
[10] C. Li, G. Xian, Mechanical property evolution and life prediction of carbon fiber and pultruded carbon fiber reinforced polymer plate exposed to elevated temperatures, Polym. Compos. 41 (2020) 5143–5155, https://doi.org/10.1002/pc.25782.
[11] D. Zhao, T.Q. Liu, X. Lu, X. Meng, Experimental and numerical analysis of a novel curved sandwich panel with pultruded GFRP strip core, Compos. Struct. 288 (2022), 115404, https://doi.org/10.1016/j.compstruct.2022.115404.
[12] J. Haloi, S.K. Mushahary, A.C. Borsaikia, K.D. Singh, Experimental investigation on the web crippling behaviour of pultruded GFRP wide-flange sections subjected to two-flange loading conditions, Compos. Struct. 259 (2021), 113469, https://doi.org/10.1016/j.compstruct.2020.113469.
[13] M. Ueda, N. Ui, A. Ohtani, Lightweight and anti-corrosive fiber reinforced thermoplastic rivet, Compos. Struct. 188 (2018) 356–362, https://doi.org/10.1016/j.compstruct.2018.01.040.
[14] K. Minchenkov, A. Vedernikov, A. Safonov, I. Akhatov, Thermoplastic pultrusion: a review, Polymers (Basel) 13 (2021) 1–36, https://doi.org/10.3390/polym13020180.
[15] S. Suresh, V.S. Senthil Kumar, Effects of fabric structure on the formability characteristics of thermoplastic composites under various process conditions, Trans. Can. Soc. Mech. Eng. 42 (2018) 298–308, https://doi.org/10.1139/tcsme-2017-0075.
[16] M.R. Choudhury, K. Debnath, A review of the research and advances in electromagnetic joining of fiber-reinforced thermoplastic composites, Polym. Eng. Sci. 59 (2019) 1965–1985, https://doi.org/10.1002/pen.25207.
[17] G.A. Vincent, T.A. de Bruijn, S. Wijskamp, M. van Drongelen, R. Akkerman, Process- and material-induced heterogeneities in recycled thermoplastic composites, J. Thermoplast. Compos. Mater. 35 (12) (2022) 2530–2551, https://doi.org/10.1177/0892705720979347.
[18] S.S. Yao, F.L. Jin, K.Y. Rhee, D. Hui, S.J. Park, Recent advances in carbon-fiber-reinforced thermoplastic composites: a review, Compos. B Eng. 142 (2018) 241–250, https://doi.org/10.1016/j.compositesb.2017.12.007.
[19] K. Minchenkov, A. Vedernikov, Y. Kuzminova, S. Gusev, A. Sulimov, A. Gulyaev, A. Kreslavskaya, I. Prosyanoy, G. Xian, I. Akhatov, A. Safonov, Effects of the quality of pre-consolidated materials on the mechanical properties and morphology of

thermoplastic pultruded flat laminates, Compos. Commun. 35 (2022) 101281, https://doi.org/10.1016/j.coco.2022.101281.
[20] N. Svensson, R. Shishoo, M. Gilchrist, Manufacturing of thermoplastic composites from commingled yarns - a review, J. Thermoplast. Compos. Mater. 11 (1998) 22–56, https://doi.org/10.1177/089270579801100102.
[21] P.J. Novo, J.P. Nunes, J.F. Silva, V. Tinoco, A.T. Marques, Production of thermoplastics matrix preimpregnated materials to manufacture composite pultruded profiles, Cienc e Tecnol Dos Mater 25 (2013) 85–91, https://doi.org/10.1016/j.ctmat.2014.03.004.
[22] Tucci F, Rubino F, Pasquino G, Carlone P. Thermoplastic Pultrusion Process of Polypropylene/Glass Tapes. Polymers (Basel) 2023;15:2374. https://doi.org/10.3390/polym15102374.
[23] O. Alajarmeh, X. Zeng, T. Aravinthan, T. Shelley, M. Alhawamdeh, A. Mohammed, L. Nicol, A. Vedernikov, A. Safonov, P. Schubel, Compressive behaviour of hollow box pultruded FRP columns with continuous-wound fibres, Thin-Walled Struct. 168 (2021) 108300, https://doi.org/10.1016/j.tws.2021.108300.
[24] A. Vedernikov, F. Tucci, P. Carlone, S. Gusev, S. Konev, D. Firsov, I. Akhatov, A. Safonov, Effects of pulling speed on structural performance of L-shaped pultruded profiles, Compos. Struct. 255 (2021) 112967, https://doi.org/10.1016/j.compstruct.2020.112967.
[25] I. Baran, R. Akkerman, J.H. Hattel, Modelling the pultrusion process of an industrial L-shaped composite profile, Compos. Struct. 118 (2014) 37–48, https://doi.org/10.1016/j.compstruct.2014.07.018.
[26] F. Ascione, G. Mancusi, S. Spadea, M. Lamberti, F. Lebon, A. Maurel-Pantel, On the flexural behaviour of GFRP beams obtained by bonding simple panels: an experimental investigation, Compos. Struct. 131 (2015) 55–65, https://doi.org/10.1016/j.compstruct.2015.04.039.
[27] T.J. Chotard, J. Pasquiet, M.L. Benzeggagh, Residual performance of scarf patch-repaired pultruded shapes initially impact damaged, Compos. Struct. 53 (2001) 317–331, https://doi.org/10.1016/S0263-8223(01)00016-2.
[28] X. Yang, Y. Bai, F.J. Luo, X.L. Zhao, F. Ding, Dynamic and fatigue performances of a large-scale space frame assembled using pultruded GFRP composites, Compos. Struct. 138 (2016) 227–236, https://doi.org/10.1016/j.compstruct.2015.11.064.
[29] J. Jeong, Y.H. Lee, K.T. Park, Y.K. Hwang, Field and laboratory performance of a rectangular shaped glass fiber reinforced polymer deck, Compos. Struct. 81 (2007) 622–628, https://doi.org/10.1016/j.compstruct.2006.12.013.
[30] S. Barros da, A. Santos Neto, H. Lebre La Rovere, Flexural stiffness characterization of fiber reinforced plastic (FRP) pultruded beams, Compos. Struct. 81 (2007) 274–282, https://doi.org/10.1016/j.compstruct.2006.08.016.
[31] M.F. Sá, A.M. Gomes, J.R. Correia, N. Silvestre, Flexural creep response of pultruded GFRP deck panels: proposal for obtaining full-section viscoelastic moduli and creep coefficients, Compos. B Eng. 98 (2016) 213–224, https://doi.org/10.1016/j.compositesb.2016.05.026.
[32] J.T. Mottram, Short- and long-term structural properties of pultruded beam assemblies fabricated using adhesive bonding, Compos. Struct. 25 (1993) 387–395, https://doi.org/10.1016/0263-8223(93)90186-T.
[33] D.J. Kwon, J.H. Kim, S.M. Park, I.J. Kwon, K.L. DeVries, J.M. Park, Damage sensing, mechanical and interfacial properties of resins suitable for new CFRP rope for elevator applications, Compos. B Eng. 157 (2019) 259–265, https://doi.org/10.1016/j.compositesb.2018.08.049.
[34] C. Colombo, L. Vergani, Experimental and numerical analysis of a bus component in composite material, Compos. Struct. 92 (2010) 1706–1715, https://doi.org/10.1016/j.compstruct.2009.12.012.
[35] M. Volk, S. Arreguin, P. Ermanni, J. Wong, C. Bar, F. Schmuck, Pultruded thermoplastic composites for high voltage insulator applications, IEEE Trans. Dielectr. Electr. Insul. 27 (2020) 1280–1287, https://doi.org/10.1109/TDEI.2020.008724.
[36] L.Z. Linganiso, R. Bezerra, S. Bhat, M. John, R. Braeuning, R.D. Anandjiwala, Pultrusion of flax/poly(lactic acid) commingled yarns and nonwoven fabrics, J. Thermoplast. Compos. Mater. 27 (2014) 1553–1572, https://doi.org/10.1177/0892705713486137.
[37] A. Vedernikov, K. Minchenkov, S. Gusev, A. Sulimov, P. Zhou, C. Li, G. Xian, I. Akhatov, A. Safonov, Effects of the pre-consolidated materials manufacturing method on the mechanical properties of pultruded thermoplastic composites, Polymers (Basel) 14 (11) (2022) 2246, https://doi.org/10.3390/polym14112246.
[38] S. Wiedmer, M. Manolesos, An experimental study of the pultrusion of carbon fiber-polyamide 12 yarn, J. Thermoplast. Compos. Mater. 19 (2006) 97–112, https://doi.org/10.1177/0892705706055448.
[39] M. Volk, J. Wong, S. Arreguin, P. Ermanni, Pultrusion of large thermoplastic composite profiles up to Ø 40 mm from glass-fibre/PET commingled yarns, Compos. B Eng. 227 (2021), 109339, https://doi.org/10.1016/j.compositesb.2021.109339.
[40] A.A. Safonov, P. Carlone, I. Akhatov, Mathematical simulation of pultrusion processes: a review, Compos. Struct. 184 (2018) 153–177, https://doi.org/10.1016/j.compstruct.2017.09.093.
[41] G. Sala, D. Cutolo, The pultrusion of powder-impregnated thermoplastic composites, Compos. A Appl. Sci. Manuf. 28 (1997) 637–646, https://doi.org/10.1016/S1359-835X(97)00002-X.
[42] A.H. Miller, N. Dodds, J.M. Hale, A.G. Gibson, High speed pultrusion of thermoplastic matrix composites, Compos. A Appl. Sci. Manuf. 29 (1998) 773–782, https://doi.org/10.1016/S1359-835X(98)00006-2.
[43] D.H. Kim, L.W. Il, K. Friedrich, A model for a thermoplastic pultrusion process using commingled yarns, Compos. Sci. Technol. 61 (2001) 1065–1077, https://doi.org/10.1016/S0266-3538(00)00234-7.
[44] S. Koubaa, C. Burtin, S. Lecorre, A. Poitou, Simple modelling of impregnation in pultrusion process of thermoplastic composites, Int. J. Microstruct. Mater. Prop. 7 (2012) 428–438, https://doi.org/10.1504/IJMMP.2012.050945.
[45] A. Carlsson, B.T. Astrom, Modelling of heat transfer and crystallization kinetics in thermoplastic composites: pultrusion, Polym. Compos. 18 (1998) 1324–1334, https://doi.org/10.1002/pc.10108.
[46] B.T. Åstroöm, R.B. Pipes, A modeling approach to thermoplastic pultrusion. I: formulation of models, Polym. Compos. 14 (1993) 173–183, https://doi.org/10.1002/pc.750140303.
[47] A. Babeau, S. Comas-Cardona, C. Binetruy, G. Orange, Modeling of heat transfer and unsaturated flow in woven fiber reinforcements during direct injection-pultrusion process of thermoplastic composites, Compos. A Appl. Sci. Manuf. 77 (2015) 310–318, https://doi.org/10.1016/j.compositesa.2015.04.017.
[48] I. Baran, J.H. Hattel, R. Akkerman, C.C. Tutum, Mechanical modelling of pultrusion process: 2D and 3D numerical approaches, Appl. Compos. Mater. 22 (2015) 99–118, https://doi.org/10.1007/s10443-014-9394-3.
[49] P. Carlone, G.S. Palazzo, Viscous pull force evaluation in the pultrusion process by a finite element thermo-chemical rheological model, Int. J. Mater. Form. 1 (2008) 831–834, https://doi.org/10.1007/s12289-008-0264-0.
[50] Ushakov A, Klenin Y, Sorina T, Khrulenko M, Solov'ev A. Physical and mechanical propeties of composite material based on thermoplastic tapes reinforced with continuous fibers. Russ. Sci. Tech. Conf. "Thermoplastic Mater. Funct. Cover., Moscow: n.d., p. 215–24.
[51] I. Baran, C.C. Tutum, M.W. Nielsen, J.H. Hattel, Process induced residual stresses and distortions in pultrusion, Compos. B Eng. 51 (2013) 148–161, https://doi.org/10.1016/j.compositesb.2013.03.031.
[52] R.M. Hackett, S.Z. Zhu, Two-dimensional finite element model of the pultrusion process, J. Reinf. Plast. Compos. 11 (1992) 1322–1351, https://doi.org/10.1177/073168449201101201.
[53] P.J. Novo, J.F. Silva, J.P. Nunes, A.T. Marques, Pultrusion of fibre reinforced thermoplastic pre-impregnated materials, Compos. B Eng. 89 (2016) 328–339, https://doi.org/10.1016/j.compositesb.2015.12.026.
[54] A. Carlsson, Å.B. Tomas, Experimental investigation of pultrusion of glass fibre reinforced polypropylene composites, Compos. A Appl. Sci. Manuf. 29 (1998) 585–593, https://doi.org/10.1016/S1359-835X(97)00115-2.
[55] I. Baran, C.C. Tutum, J.H. Hattel, The effect of thermal contact resistance on the thermosetting pultrusion process, Compos. B Eng. 45 (2013) 995–1000, https://doi.org/10.1016/j.compositesb.2012.09.049.
[56] A. Safonov, M. Gusev, A. Saratov, A. Konstantinov, I. Sergeichev, S. Konev, S. Gusev, I. Akhatov, Modeling of cracking during pultrusion of large-size profiles, Compos. Struct. 235 (2020) 111801, https://doi.org/10.1016/j.compstruct.2019.111801.
[57] Moplen RP348U. n.d. http://img9.cntrades.com/201603/23/16-02-57-18-1009588.pdf (accessed September 9, 2022).
[58] P. Esfandiari, J.F. Silva, P.J. Novo, J.P. Nunes, A.T. Marques, Production and processing of pre-impregnated thermoplastic tapes by pultrusion and compression moulding, J. Compos. Mater. 56 (11) (2022) 1667–1676, https://doi.org/10.1177/00219983221083841.
[59] A. Safonov, S. Gusev, M. Rubtsov, I. Sergeichev, I. Akhatov, Thermoplastic pultrusion reinforcement insert in a hollow plastic frame of a window or door unit, RU2738062C1 (2020).
[60] C. Ageorges, L. Ye, M. Hou, Advances in fusion bonding techniques for joining thermoplastic matrix composites: a review, Compos - Part A Appl Sci Manuf 32 (2001) 839–857, https://doi.org/10.1016/S1359-835X(00)00166-4.
[61] A. Vedernikov, A. Safonov, F. Tucci, P. Carlone, I. Akhatov, Modeling spring-in of l-shaped structural profiles pultruded at different pulling speeds, Polymers (Basel) (2021) 13, https://doi.org/10.3390/polym13162748.
[62] I. Baran, J.H. Hattel, R. Akkerman, Investigation of process induced warpage for pultrusion of a rectangular hollow profile, Compos. B Eng. 68 (2015) 365–374, https://doi.org/10.1016/j.compositesb.2014.07.032.